Solar Water Splitting

A Stable Integrated Photoelectrochemical Reactor for H₂ Production from Water Attains a Solar-to-Hydrogen Efficiency of 18 % at 15 Suns and 13 % at 207 Suns

Mohd A. Khan, Ibraheam Al-Shankiti, Ahmed Ziani, Nimer Wehbe, and Hicham Idriss*

Abstract: *The major challenge in solar water splitting to H₂ and O₂ is in making a stable and affordable system for large-scale applications. We have designed, fabricated, and tested a photoelectrochemical reactor characterized as follows: 1) it comprises an integrated device to reduce the balance of the system cost, 2) it utilizes concentrated sunlight to reduce the photoabsorber cost, and 3) it employs and alkaline electrolyte to reduce catalyst cost and eliminate external thermal management needs. The system consists of an III-V-based photovoltaic cell integrated with Ni foil as an O₂ evolution catalyst that also protects the cell from corrosion. At low light concentration, without the use of optical lenses, the solar-to-hydrogen (STH) efficiency was 18.3 %, while at high light concentration (up to 207 suns) with the use of optical lenses, the STH efficiency was 13 %. Catalytic tests conducted for over 100 hours at 100–200 suns showed no sign of degradation nor deviation from product stoichiometry (H₂/O₂ = 2). Further tests projected a system stability of years.*

Introduction

Hydrogen is an important raw material for chemical and refinery industries, which is primarily used for the production of ammonia and methanol, and secondly for hydrotreating in refineries.[1] Presently, almost half of the world's population depends on food made from ammonia-based fertilizer,[2] making the availability of low-cost hydrogen a critical issue. Moreover, hydrogen may play a future role in the energy sector and in conversion of CO_2 into useful fuels and chemicals. Currently, steam methane reforming (SMR) is the most widely used process for H₂ production with a cost of approximately 0.8–2.0 \$ kg⁻¹ H₂ (without accounting for carbon capture, use, and storage (CCUS)), depending on geographic location.[3–5] A major drawback of the SMR process are the CO_2 emissions. Dependent on the nature of feedstock (natural gas, rich gases, naphtha, and so on), one ton of hydrogen simultaneously produces 8 to 12 tons of CO_2 (the weight ratio of CO_2 to H₂ produced by the combined processes of SMR and the water–gas shift reaction is 5.5).[6]

Solar-driven water splitting is a clean and sustainable route for H₂ production and it has been the subject of intense research efforts over the last few decades.[7–9] Photovoltaic (PV)–electrolysis systems that use PV modules connected physically and electrically in series with electrolyzers present the most mature technology for solar H₂ production. There are several relatively small-scale demonstrations of PV–electrolysis systems with more than 15 % solar-to-hydrogen (STH) efficiency.[10–12] However, the use of power electronics and a significant number of other auxiliary control components leads to a high balance of system (BOS) cost. This increases the cost of H₂ production and the latest techno-economic studies indicate that PV–electrolysis will result in a H₂ cost between 5 and 15 \$ kg⁻¹, depending on the PV technology and location.[13,14] While this progress is promising, it is very challenging to compete with SMR technology in terms of cost.

For this reason, photoelectrochemical (PEC) systems that integrate the photoabsorber (as a multijunction high-concentration solar cell) with catalysts provide an opportunity for the necessary cost reduction.[8,15] However, there are several challenges associated with developing practical PEC systems for industrial scale H₂ production. PEC devices are less developed and have efficiencies lower than PV–electrolysis systems.[8,16] This is because of their instability in harsh electrolytes.[17–19] Another development challenge is to scale up these PEC devices so as to reach the same H₂ production capacity as that of the PV–electrolysis system. Therefore, high efficiencies are not the sole target, but high power and cell-current densities are needed. These would allow reductions in the size of the PEC elements, and consequently, a decrease in the cost of hydrogen produced over the device lifetime.[20,21] This can be achieved by increasing photocurrents under concentrated light. However, working at elevated operating current densities bring other complexities given the significant increase in temperature and overpotential, which exacerbate degradation of the photoabsorber and catalysts.[21–23]

[*] M. A. Khan, I. Al-Shankiti, A. Ziani, H. Idriss
Hydrogen Platform
SABIC-Corporate Research and Development (CRD) center
King Abdullah University of Science and Technology (KAUST)
Thuwal (Saudi Arabia)
E-mail: IdrissH@SABIC.com

N. Wehbe
Imaging & Characterization Core Lab
King Abdullah University of Science and Technology (KAUST)
Thuwal (Saudi Arabia)

Supporting information and the ORCID identification number(s) for the author(s) of this article can be found under:
https://doi.org/10.1002/anie.202002240.

In one of the earliest reports on developing PEC reactors for operation under high (> 100 suns) concentrated light, Peharz and co-workers[24] developed a reactor for water splitting at approximately 500 kW m^{-2}. The system consisted of a III–V multijunction cell coupled externally with a proton exchange membrane (PEM) electrolyzer. While the reactor had a high STH efficiency of about 15%, the reported stability was for a few of hours. To calculate the STH, the authors assumed that all energy needed to split water comes from electricity because of the high current density; in this case the thermoneutral potential of 1.48 V per H atom was used for the efficiency calculation (285 kJ mol^{-1} at 1 bar, 25°C, 2.39 kWh kg^{-1}). Furthermore, the system was designed using expensive current collectors, flow plates, and catalysts. Recently Haussener and co-workers[25] reported a PEC reactor for water splitting at 474 kW m^{-2} with a STH efficiency of 15%. The experiment was conducted using a high-power solar simulator (that is, without the use of optical concentrators) but the reported stability was for a few minutes. Furthermore, the use of a copper cooling plate and titanium flow plate would increase the cost of the reactor. There have also been a few reports[26–31] on the use of lower sun concentrations (2 to 42 suns) for H$_2$ production, but again, with maximum reported stabilities of a few hours.

Herein, we address these combined challenges and demonstrate a PEC hydrogen reactor that works under high concentrated light. We propose a design that allows the reactor to perform at high efficiency and is at the same time stable. Firstly, we have directly integrated the III–V-based PV cell with the oxygen evolution reaction (OER) catalyst to avoid ohmic losses that can potentially reduce the efficiency

of the system. This also helped to eliminate expensive current collector components, as used in previous reports.[24,25] Secondly, we worked with an alkaline electrolyte to avoid using expensive OER catalysts, thereby allowing for a non-zero gap configuration as opposed to PEM-based systems. The design also used the electrolyte to cool the PV cell, therefore eliminating the need for external thermal management.[25] Equally important, the reactor was designed in such a way to ensure that the PV cell is isolated from the electrolyte, and thereby protecting it from possible corrosion. Without the contribution of optical losses from Fresnel lens, we were able to reach close to maximum theoretical STH efficiency at approximately 18.3 ± 0.7% under light fluxes of 10 kW m^{-2} and 15 kW m^{-2}. At higher light flux up to 207 kW m^{-2}, we reached photocurrent densities up to 2.24 A cm^{-2} and associated H$_2$ production rates of approximately 3.10 mL min^{-1}, corresponding to 13% ± 0.6% STH efficiency. The decrease in STH is a consequence of optical loss upon using the Fresnel lenses and is independent of sun concentration. Constant H$_2$ and O$_2$ production with time, and with a ratio equal to 2, is an indication of system stability.

Results and Discussion

Figure 1a presents the PV characteristics of the GaInP/GaInAs/Ge triple junction (3J) PV cell under 1, 10, and 15 suns, respectively, without the use of the optical concentrator (that is, the Fresnel lens). The solar light flux was obtained by adjusting the distance and power of the solar simulator, and calibrated using a silicon photodetector, as described in the
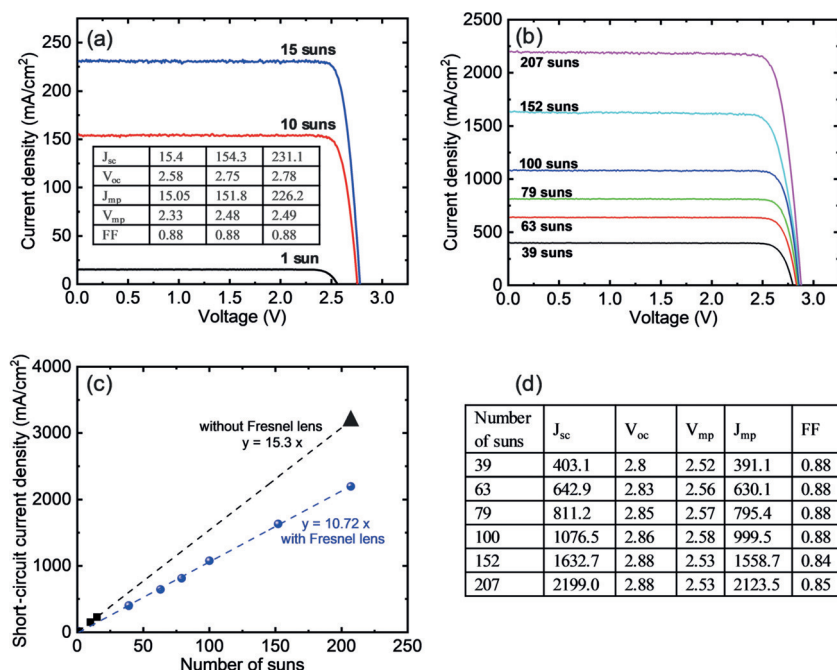
Figure 1. a) PV characteristics of the GaInP/GaInAs/Ge PV cell under concentrated light without the use of a Fresnel lens. b) PV characteristics of the GaInP/GaInAs/Ge PV cell under concentrated light with the use of a Fresnel lens. c) Short-circuit current density (J_{sc}) as a function of the number of suns with (●) and without (■) the use of a Fresnel lens. The difference in the slope of both lines indicates losses arising from use of the Fresnel lens (ca. 30%). An extrapolated linear point as a visual guide (▲). d) Summary of PV characteristics shown in (b).

Experimental Section. Under 1 sun, the short-circuit current density (J_{sc}), the open-circuit voltage (V_{oc}), maximum power current density (J_{mp}), maximum power voltage (V_{mp}), and fill factor (FF) were 15.4 mA cm^{-2}, 2.58 V, 15.05 mA cm^{-2}, 2.33 V, and 0.88, respectively. Practical solar light concentration is achieved using either parabolic mirrors or Fresnel lenses, which focus the light onto smaller area light absorbers.[32] Figure 1b displays the PV characteristics of the GaInP/GaInAs/Ge/Au 3J cell under concentrated light coming from a poly(methyl methacrylate) (PMMA) Fresnel lens (area A_1 ≈ 19.6 cm^2; see Figures 4a–c in the Experimental Section for depictions of the PEC reactor). The concentrated light spot had a diameter of roughly 0.5 cm; thus, the spot size area A_2 was approximately 0.196 cm^2, leading to a geometric concentration ratio of 100. By controlling the light intensity incident on the Fresnel lens (0.39, 0.63, 0.79, 1.0, 1.52, and 2.07 suns) light fluxes of 39, 63, 79, 100, 152, and 207 suns were thus obtained, respectively.

Under uniform irradiance and constant temperature, the short-circuit current density is considered linear with respect to light concentration, as expressed in Equation (1):[23]

$$J_{sc} = X J_{sc-1sun} \tag{1}$$

where X is the light concentration factor, and $J_{sc-1sun}$ is the short-circuit current density at one sun (1 kW m^{-2}). While there is a linear increase of J_{sc} as a function of light concentration (Figure 1c), the use of Fresnel lens leads to optical losses of about 30%, as indicated by the difference in slope of the two curves in Figure 1c (for a detailed calculation of optical losses, see the Supporting Information, Table S1). The PV characteristics are summarized in Figure 1d. There is a small drop in FF at high concentrations that we attribute to the non-uniform light flux (Supporting Information, Figure S2). The concentrated light from the Fresnel lens has a non-uniform Gauss-like intensity distribution resulting in a decreased FF.[33,34]

Results of the integrated PEC reactor under concentrated light are presented in Figure 2. The first set of experiments were carried out without using an anion exchange membrane (AEM). The electrolyte (5 M KOH) was flowed into the reactor from one side only and the H$_2$/O$_2$ gases were collected together in a single eudiometer. Figure 2a presents the combined H$_2$ and O$_2$ production rates, which increased linearly as a function of light concentration. We have also measured, in parallel, the activity at 100 suns using different concentrations of KOH (0.5, 1, and 5 M) and flow rates (2 to 40 mL min^{-1}); both showed marginal effect, within experimental errors (Supporting Information, Figure S3).

Upon incorporating the alkaline membrane directly on top of the Pt/Ti mesh, and keeping all other reactor components unchanged, H$_2$ and O$_2$ gases were collected separately in two different eudiometers. The H$_2$ production rates were initially checked by gas chromatography (GC) measurements to remove any errors arising from water vapor (water partial pressure at 25°C is about 0.031 atm) and possible dissolved molecular O$_2$ (Supporting Information, Note S1). GC measurements indicated that the contribution
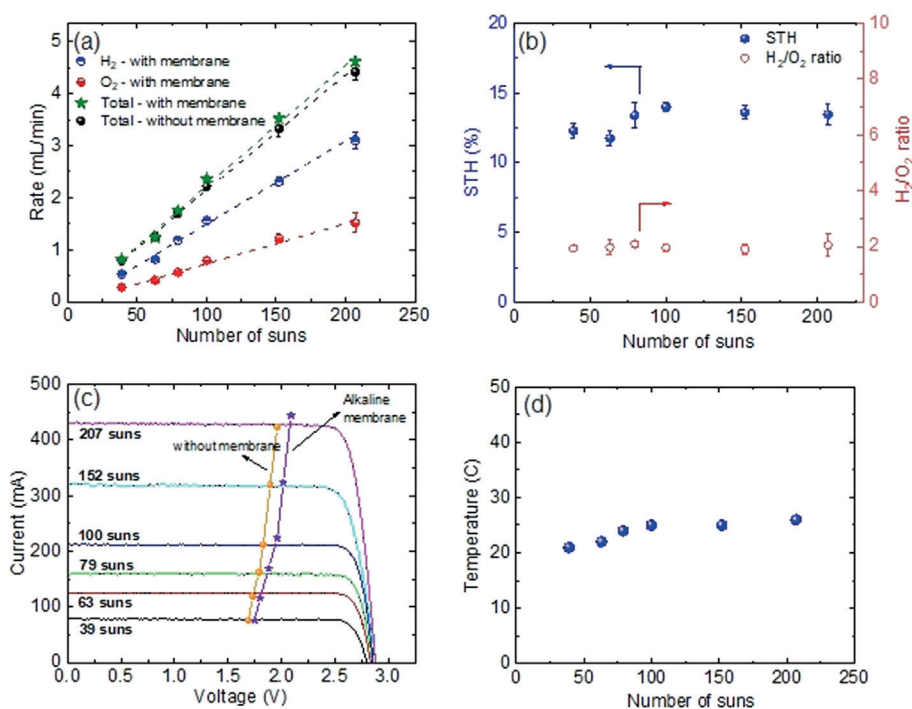
Figure 2. a) H$_2$ and O$_2$ production rates (with and without an anion exchange membrane). b) H$_2$/O$_2$ ratio and STH efficiency as a function of light concentration using an anion exchange membrane (Sustainion® 37–50); the top dashed line represents the average STH of 13%, the bottom dashed line represent the H$_2$ to O$_2$ stoichiometric ratio of 2. c) IV characteristics of the 3J GaInP/GaInAs/Ge cell overlapped with H$_2$ production rates (a) converted to the corresponding current values (Supporting Information, Note S3). Electrolyte = 5 M KOH, flow rate = 8 mL min^{-1}. d) Cell temperature measured during the reaction at the given sun concentration.

of water vapor into the volumetric measurement was negligible and no crossing of molecular O_2 was observed into the H_2 side. H_2 and O_2 production rates increased linearly as a function of light concentration (Figure 2a). The reaction at each light concentration was carried out for a total of 2 hours with five separate measurements for H_2 and O_2 rates. The STH efficiencies (Figure 2b) were calculated using Equation (2) after each measurement, and the error bars were calculated at the end of the experiment based on a 95% confidence interval.

$$\text{System efficiency} = \text{STH}$$
$$= \frac{\text{Power from } H_2 \text{ produced}}{\text{Power of light incident on the Fresnel lens}} \quad (2)$$
$$= \frac{r_{H_2} \Delta G_r}{A_{PV} \Phi}$$

Where r_{H_2} is the H_2 production rate in $mol\,s^{-1}$, ΔG_r is the free energy of reaction ($H_2O \rightarrow H_2 + \frac{1}{2}O_2$; $237\,000\,J\,mol^{-1}$), A_{PV} is the PV cell area (cm^2), and Φ is the light flux ($J\,s^{-1}\,cm^{-2}$).

The H_2/O_2 ratio of 2:1, as shown in Figure 2b, indicates a stable system. The average STH efficiency at different light concentrations was found to be approximately $13 \pm 0.7\%$. An example of how the system efficiency for 100 suns was calculated is given in Note S2 of the Supporting Information. The maximum possible STH efficiency upon using these PV cells is about 18.8% based on a faradaic efficiency (η_F) of 100%. The drop in STH is a result of 30% optical losses coming from the Fresnel lens (Figure 1c). This was confirmed by performing experiments under low concentrations (10 and 15 suns) without the use of a Fresnel lens (for which an STH efficiency of 18.3% was obtained; Supporting Information, Figure S4).

The H_2 production rates upon incorporating a membrane were identical to the case without using it. The use of a membrane introduces some resistance because $V_{mp} > E_{cell}$ H_2 production is not affected. This is evident in Figure 2c, where we overlap the PV cell performance of Figure 1b and PEC device performance of Figure 2a. The PV cell performance was plotted as current versus voltage so that it can be plotted together with the PEC data. The voltage of the PEC device was measured under incident concentrated light and the H_2 produced was converted into current (Supporting Information, Note S3). From Figure 2c we observe that the H_2 produced is very close to J_{sc} from the PV cell, indicating faradaic efficiencies of about 100%. Furthermore, the difference in performance of the PEC reactor with and without membrane is seen by the increase in required voltage for the catalytic reaction. The resistance calculated from difference in voltage (ΔV) and current (I_{sc}) is in the range of 0.5–0.7 Ω for the various light concentrations. It is important to mention that, while we are not operating at the maximum power point (MPP), the H_2 production rates and efficiency are dictated by the I_{sc}. Optimizing the catalyst amount to operate at MPP does not increase the H_2 production rate or efficiency in an integrated PEC system.[35] On the contrary, decreasing the catalyst amount to operate at MPP might be detrimental for the stability of the catalyst and increases risk of drop in

efficiency over time. This extra voltage can be utilized in a decoupled PV–electrolysis setup using a DC–DC converter. However, the use of a DC–DC converter and corresponding electronics increases the BOS cost. Figure 2d presents the recorded temperature of the cell under working conditions using a thermocouple at the edge of the cell. The recorded temperature was about 30°C. Good thermal management is supported by the PV characteristics (Figure 1), a linear increase in current, and logarithmic increase in voltage with increasing sun concentration. An increase in cell temperature would have resulted in a deviation from this behavior.

Figure 3a displays the long-term stability data of the integrated PEC reactor under alternating 100 and 200 suns light fluxes. The PEC reactor showed stable performance with constant H_2/O_2 production (ratio of 2:1) at a STH efficiency of approximately 13% for the duration of the test without degradation, which is the highest reported stability for PEC H_2 production under concentrated light. The reactor demonstrated good thermal management at high operating photocurrents. Any potential failure of the system would be
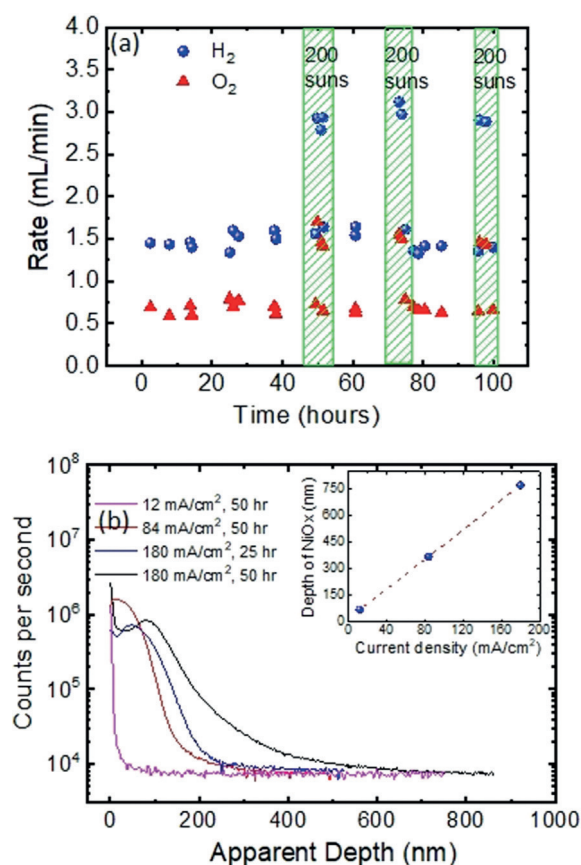
Figure 3. a) Stability tests of integrated PEC reactor under alternating 100 and 200 suns light flux using a Fresnel lens together with H_2 and O_2 production rates plotted as a function of time. The green shaded area shows the data when operating under 200 suns. The current density at 200 suns is 107.5 $mA\,cm^{-2}$. b) Depth profile of the Ni surface where the $^{90}NiO_x^-$ secondary ion signal was monitored after the electrochemical oxidation reaction. Inset: the oxide layer thickness measured from the SIMS experiment plotted against electrochemical current density.

because of a leak into the seal, which is a manufacturing rather than a conceptual issue.

While stoichiometric H_2/O_2 production indicates true water splitting,[36] the role of the Ni catalyst in protecting the 3J PV cell from the electrolyte needed further study. For this purpose, the Ni surface was analyzed using dynamic secondary ion mass spectrometry (SIMS). The Ni foil was subjected to electrochemical oxidation in conditions similar to those of the PEC tests under different current densities. Figure 3b displays the depth profile of the Ni surface, where the $^{90}NiO_x^-$ secondary ion signal was monitored. The point at which the signal from the $^{90}NiO_x^-$ secondary ion fragment becomes constant represents the oxide/bulk Ni interface. SIMS results indicate that the oxide layer thickness increases linearly with time at constant current; see for example the difference between 25 and 50 hour samples at 180 mA cm^{-2}. From these data, the rate of Ni oxidation can be extracted and is found to be 0.088 nm per mA cm^{-2} per hour. This oxidation rate is negligible and does not disturb the stoichiometry of H_2/O_2 (Supporting Information, Table S2). To confirm Ni oxidation is an electrochemical process we have also carried out SIMS depth profiling of Ni dipped in alkaline electrolyte under dark conditions, and no oxidation with time was seen (Supporting Information, Figure S5). The results highlight that, when working under concentrated light (higher currents), it would be better to dilute the photocurrents from the PV cell onto a larger area catalyst, not only to maximize efficiency[21] but also for longer stability of the catalysts.

For long-term stability projections, the oxidation rate derived from the SIMS experiment at 0.088 nm per mA cm^{-2} per hour may be used to calculate the expected stability of such systems. For example, under 200 suns, with a photocurrent of 430 mA, and an electrochemical current density of 107.5 mA cm^{-2} (4 cm^2 area Ni in our PEC reactor), the oxidation time for a 250 μm thick Ni layer may be calculated to approximately 9.1 years based on 8 hours of daily operation. This number can be taken as a projection for commercial use. Accelerated stability tests, for example, at a much higher concentration of 1000 suns, are needed for further verification.

Conclusion

Herein, we have presented a PEC reactor for H_2 production from water that operates under concentrated sunlight close to the maximum theoretical efficiency (ca. $18.3 \pm 0.7\%$) at low light flux (10 and 15 suns). Under higher light flux, obtained using a Fresnel lens, H_2 production rates linearly increased at a constant STH efficiency of approximately $13 \pm 0.6\%$, reaching 3.10 mL min^{-1} at 207 suns (short-circuit current density = 2.24 A cm^{-2}, electrochemical current density = 107.5 mA cm^{-2}). The reactor was stable with a stoichiometric H_2/O_2 ratio for the duration of the tests (>100 hours) with an extrapolated lifetime of >9 years. The development of active and stable integrated PEC reactors with H_2/O_2 separation may represent a step forward toward the realization of "green" hydrogen with affordable cost. Because the system works well in an alkaline environ-

ment using Ni-based catalysts, an excess amount of catalyst with respect to cell area would be beneficial,[37] since the determining geometric factor is that of the total sunlight area before concentration. Therefore, working with low electrochemical current density ensures stability while producing the same amount of H_2. The H_2 production rate and STH efficiency of such systems can be improved by optimizing the growth/performance of III–V PV cells to obtain a maximum cell current density and optimal V_{mp} (ca. 1.8–2.0 V) for solar water splitting. The optical losses under concentrated light can also be reduced ($<20\%$) by selecting an appropriate Fresnel lens similar to that in commercial concentrator PV (CPV) modules. With the development of such reactors, the design of large-scale PEC modules and techno-economics studies (Supporting Information, Note S3), similar to that for CPV–electrolysis[38] are needed. Moreover, it is necessary to address the long-term stability of the membranes (stability of many years is required), as well as that of the different components of the electrodes. Moreover, assessment of safety hazards associated with use of a KOH base in a much larger plumbing and distribution system needs to be compared to that of a MW-scale conventional alkaline electrolyzer stack.

Experimental Section

PEC reactor fabrication. Figures 4a and b present a schematic and illustration of the integrated PEC reactor designed for use under concentrated light. The reactor was fabricated using a transparent PMMA ideal for use in alkaline conditions (pH $\approx$ 14). A 3J GaInP/GaInAs/Ge PV cell (5.0×5.0 mm^2 = 0.25 cm^2) from Azure Space was used as the photoabsorber. The reactor area was 6×6 cm^2 (36 cm^2) and fabricated using a CO$_2$-based laser (Epilog Fusion M2; wavelength = 10.6μ) at a power setting of 75 W. Electrical connection from the front of the 3J PV cell was done using ball wire bonding with 25 μm gold wire (HB16, TPT Wire Bonder GmbH & Co) onto a copper foil. The back of the 3J PV cell was integrated with a 0.25 mm thick Ni foil (Alfa Aesar, 99.5% purity) using silver paste (Alfa Aesar 42469), which was cured at 60°C for 2 hours in air. The Ni geometric area was kept at approximately 4 cm^2 and the hydrogen evolution reaction (HER) catalyst used was approximately 50 nm thick Pt sputtered onto both sides of a porous titanium mesh (Goodfellow TI008710, nominal aperture = 0.19 mm, wire diameter = 0.23 mm, open area = 20%). Prior to sputtering, the Ti mesh was cleaned with 0.2 M oxalic acid for 10 min before loading into the sputter chamber. Pt was sputtered using a radio frequency (RF) sputtering method at a constant RF power of 400 W at 5 mTorr Ar pressure during deposition. The thickness of Pt was verified using a stylus profiler for a film deposited on silicon, which was kept in the sputter chamber along with the Ti mesh. An alkaline anion exchange membrane (Sustainion® 37–50, dioxide materials) with area $\approx$12.96 cm^2 was used for ion transfer and gas separation. The membrane was activated by dipping it in a 1 M KOH electrolyte solution for 12 h. Sustainion® 37–50 is a new imidazole-functionalized membrane with a polystyrene-based backbone, which is stable in strong alkaline solutions. Dioxide materials have demonstrated long-term stability in thousands of hours at high current densities (1 A cm^{-2}).[39]

PEC testing. Figure 4c shows the experimental setup for the PEC reactions. An Asahi Spectra HAL-320W solar simulator (350–1800 nm) was used as the light source. A PMMA (Edmund Optics, #43-025) Fresnel lens with an area of approximately 19.6 cm^2 was used
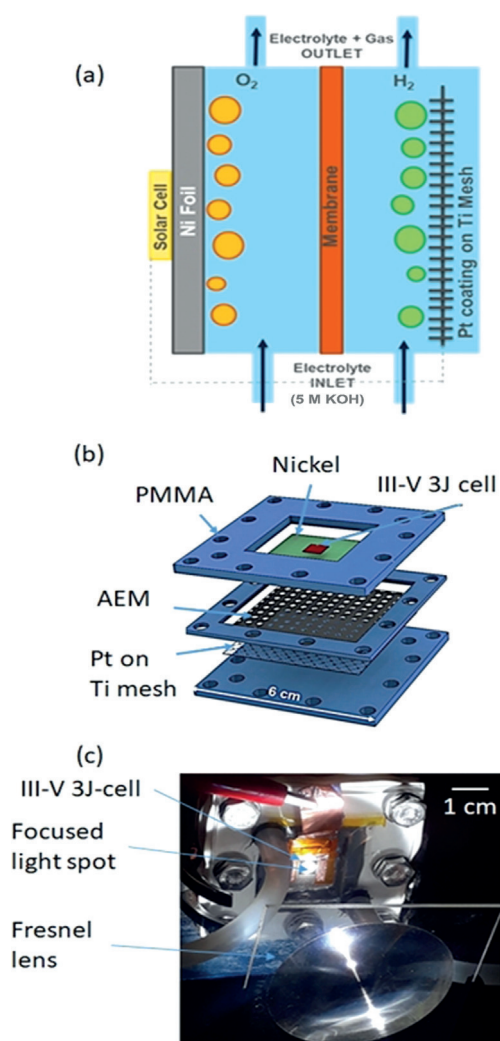
Figure 4. a) Schematic and b) illustration of the integrated PEC reactor in which the components from which the reactor is fabricated are displayed. c) Photograph of the integrated PEC reactor and Fresnel lens under illumination. The ratio A_1/A_2 of the Fresnel lens area ($A_1 = 19.6$ cm^2) and that of the focused light spot area (A_2) gives the geometric light concentration. In (a) the gap between the membrane and the Ni foil is ca. 2.5 mm, while that between the membrane and the Ti mesh is close to 1 mm.

to concentrate light onto a 3J PV cell kept at the focal distance from the lens (5 cm). The light flux was measured using a precalibrated monocrystalline silicon reference cell (Newport, 91150-KG5) and a precalibrated high concentration 3J GaInP/GaInAs/Ge reference cell (Azure space, 3C42A). The light flux measurements were further verified using a spectroradiometer (Spectral Evolution SR-500) in a range of 350–1100 nm (Supporting Information, Figure S1). For reactions performed without the use of a concentrating Fresnel lens (10 and 15 suns), the irradiation was adjusted by the distance to the PV cell and the power of the solar simulator. Specifically, the experiments conducted at 10 suns were performed at a distance of 8 cm and 60% intensity, and for 15 suns at 8 cm and 90% intensity. A peristaltic pump was used to flow 5 M KOH as the electrolyte for the reaction and the H$_2$/O$_2$ gases were collected using two separate inverted eudiometers. The total volume of the KOH in the collection system was about 0.5 L. At 5 M concentration, the solubility of O$_2$ is approximately 0.1×10^{-3} moles L bar^{-1}.[40] Thus, maximum dissolved O$_2$ at 1 atm is approximately 0.2×10^{-3} moles = 0.00892 mL O$_2$, which

is negligible when compared to the amount of O$_2$ detected. The temperature of the cell was measured at the corner with a type K thermocouple. To monitor H$_2$, a gas chromatograph (Agilent Technologies, 7890A) equipped with a thermal conductivity detector (TCD) connected to a Porapak Q packed column (2 m long, 1/8 in. external diameter) at 45°C was used with N$_2$ as the carrier gas (flow rate = 20 mL min^{-1}, pressure = 8 psi). O$_2$ was monitored using another GC (Thermo Scientific, Trace1300) equipped with a TCD connected to a packed molecular sieve (5Å) column (2 m long, 1/8 in. external diameter) with He as the carrier gas (flow rate = 1.5 mL min^{-1}, pressure = 22 psi). The complete system is available upon request.

SIMS depth profiling. Depth-profiling experiments were performed on a dynamic SIMS instrument from Hiden analytical company (Warrington-UK) operated under ultrahigh vacuum (UHV) conditions (typically 10^{-9} torr). A continuous Ar$^+$ beam of 4 keV energy was employed to sputter the surface while the selected ions were sequentially collected using a MAXIM spectrometer equipped with a quadrupole analyzer. The sputtered area is estimated to be 750×750 μm^2. To avoid the edge effect during depth-profiling experiments, it is necessary to acquire data from a small area located in the middle of the eroded region. Using an adequate electronic gating, the acquisition area was scaled down to approximately 75×75 μm^2. The conversion of the sputtering time to sputtering depth scale was carried out by measuring the depth of the crater generated at the end of the depth profiling experiment using a stylus profiler from Veeco Company, with a calculated average sputtering rate of approximately 5.5 nm min^{-1}.

The Ni samples for SIMS were prepared in a two-electrode setup with Pt as the counter electrode. The electrolyte used was 5 M KOH and was continuously purged with high-purity (99.999%) N$_2$ during the reaction. The Ni was oxidized using chronopotentiometry measurements at different currents. After measurements, Ni samples were washed with deionized water and dried with N$_2$ gas before loading into the UHV chamber for SIMS depth-profiling experiments.

Conflict of interest

The authors declare no conflict of interest.

[1] M.-R. de Valladares, *Global trends and outlook for hydrogen*, technical report for the International Energy Agency (IEA) Hydrogen Technology Collaboration Program (TCP), https://ieahydrogen.org/pdfs/Global-Outlook-and-Trends-for-Hydrogen Dec2017 WEB.aspx, **2017**.

[2] J. W. Erisman, M. A. Sutton, J. Galloway, Z. Klimont, W. Winiwarter, *Nat. Geosci.* **2008**, *1*, 636.

[3] International Energy Agency (IEA), *The Future of Hydrogen*, http://www.iea.org/publications/reports/thefutureofhydrogen/, Paris, **2019**.

[4] B. Parkinson, P. Balcombe, J. Speirs, A. Hawkes, K. Hellgardt, *Energy Environ. Sci.* **2019**, *12*, 19–40.

[5] T. E. Drennen, J. E. Rosthal, *Pathways to a hydrogen future*, Elsevier, Amsterdam, **2007**.

[6] G. Collodi, F. Wheeler, *Chem. Eng. Trans.* **2010**, *19*, 37–42.

[7] S. Chen, T. Takata, K. Domen, *Nat. Rev. Mater.* **2017**, *2*, 17050.

[8] S. Ardo, D. F. Rivas, M. A. Modestino, V. S. Greiving, F. F. Abdi, E. A. Llado, V. Artero, K. Ayers, C. Battaglia, J.-P. Becker, *Energy Environ. Sci.* **2018**, *11*, 2768–2783.

[9] J. H. Kim, D. Hansora, P. Sharma, J.-W. Jang, J. S. Lee, *Chem. Soc. Rev.* **2019**, *48*, 1908–1971.

[10] J. Jia, L. C. Seitz, J. D. Benck, Y. Huo, Y. Chen, J. W. D. Ng, T. Bilir, J. S. Harris, T. F. Jaramillo, *Nat. Commun.* **2016**, *7*, 13237.

[11] A. Nakamura, Y. Ota, K. Koike, Y. Hidaka, K. Nishioka, M. Sugiyama, K. Fujii, *Appl. Phys. Express* **2015**, *8*, 107101.

[12] S. H. Wai, Y. Ota, D. Yamashita, M. Sugiyama, K. Nishioka in *High efficiency solar to gas conversion system using concentrator photovoltaic and electrochemical cell*, Grand Renewable Energy proceedings Japan council for Renewable Energy, Japan Council for Renewable Energy, **2018**, pp. 44.

[13] M. R. Shaner, H. A. Atwater, N. S. Lewis, E. W. McFarland, *Energy Environ. Sci.* **2016**, *9*, 2354–2371.

[14] J. Hinkley, J. Hayward, R. McNaughton, R. Gillespie, A. Matsumoto, M. Watt, K. Lovegrove, *Concentrating Solar Fuels Roadmap: Final Report*, ARENA Project Solar Hybrid Fuels (3-A018), CSIRO ENERGY, Australia, **2016**.

[15] K. Horowitz, M. Woodhouse, H. Lee, G. Smestad, *Bottom-Up Cost Analysis of a High Concentration PV Module*, technical report NREL/CP-6A20-63888 prepared for the National Renewable Energy Laboratory (NREL), https://www.osti.gov/biblio/1257754, Golden, CO, **2016**; K. Horowitz, M. Woodhouse, H. Lee, G. Smestad, *AIP Conference Proceedings*, **2015**, *1679*, 100001 (1–6).

[16] T. Hisatomi, J. Kubota, K. Domen, *Chem. Soc. Rev.* **2014**, *43*, 7520–7535.

[17] J. W. Ager, M. R. Shaner, K. A. Walczak, I. D. Sharp, S. Ardo, *Energy Environ. Sci.* **2015**, *8*, 2811–2824.

[18] D. Bae, B. Seger, P. C. Vesborg, O. Hansen, I. Chorkendorff, *Chem. Soc. Rev.* **2017**, *46*, 1933–1954.

[19] S. Hu, N. S. Lewis, J. W. Ager, J. Yang, J. R. McKone, N. C. Strandwitz, *J. Phys. Chem. C* **2015**, *119*, 24201–24228.

[20] M. Dumortier, S. Haussener, *Energy Environ. Sci.* **2015**, *8*, 3069–3082.

[21] C. A. Rodriguez, M. A. Modestino, D. Psaltis, C. Moser, *Energy Environ. Sci.* **2014**, *7*, 3828–3835.

[22] Y. Liu, X. Liang, L. Gu, Y. Zhang, G.-D. Li, X. Zou, J.-S. Chen, *Nat. Commun.* **2018**, *9*, 2609.

[23] E. F. Fernández, A. J. García-Loureiro, G. P. Smestad in *Multi-junction Concentrator Solar Cells: Analysis and Fundamentals, High Concentrator Photovoltaics* (Eds.: P. Pérez-Higueras, E. Fernández), Springer, Heidelberg, **2015**, pp. 9–37.

[24] G. Peharz, F. Dimroth, U. Wittstadt, *Int. J. Hydrogen Energy* **2007**, *32*, 3248–3252.

[25] S. Tembhurne, F. Nandjou, S. Haussener, *Nat. Energy* **2019**, *4*, 399.

[26] K. Walczak, Y. Chen, C. Karp, J. W. Beeman, M. Shaner, J. Spurgeon, I. D. Sharp, X. Amashukeli, W. West, J. Jin, *ChemSusChem* **2015**, *8*, 544–551.

[27] M. R. Shaner, K. T. Fountaine, S. Ardo, R. H. Coridan, H. A. Atwater, N. S. Lewis, *Energy Environ. Sci.* **2014**, *7*, 779–790.

[28] O. Khaselev, J. A. Turner, *Science* **1998**, *280*, 425–427.

[29] K. Fujii, S. Nakamura, M. Sugiyama, K. Watanabe, B. Bagheri, Y. Nakano, *Int. J. Hydrogen Energy* **2013**, *38*, 14424–14432.

[30] C. Liu, J. Tang, H. M. Chen, B. Liu, P. Yang, *Nano Lett.* **2013**, *13*, 2989–2992.

[31] J. H. Park, A. J. Bard, *Electrochem. Solid-State Lett.* **2006**, *9*, E5–E8.

[32] W. Xie, Y. Dai, R. Wang, K. Sumathy, *Renewable Sustainable Energy Rev.* **2011**, *15*, 2588–2606.

[33] V. Andreev, V. Grilikhes, V. Rumyantsev, N. Timoshina, M. Shvarts, *Effect of nonuniform light intensity distribution on temperature coefficients of concentrator solar cells*, 3rd World Conference on Photovoltaic Energy Conversion, 2003. Proceedings of IEEE, Osaka, **2003**, pp. 881–884 Vol.1..

[34] H. Baig, K. C. Heasman, T. K. Mallick, *Renewable Sustainable Energy Rev.* **2012**, *16*, 5890–5909.

[35] S. Rau, S. Vierrath, J. Ohlmann, A. Fallisch, D. Lackner, F. Dimroth, T. Smolinka, *Energy Technol.* **2014**, *2*, 43–53.

[36] M. A. Khan, P. Varadhan, V. Ramalingam, H.-C. Fu, H. Idriss, J.-H. He, *ACS Energy Lett.* **2019**, *4*, 2712–2718.

[37] S. M. Bashir, M. A. Nadeem, M. Al-Oufi, M. Al-Hakami, T. T. Isimjan, H. Idriss, *ACS Omega* **2020**, *5*, 10510–10518.

[38] S. O. Alsayegh, R. Varjian, Y. Alsalik, K. Katsiev, T. T. Isimjan, H. Idriss, *ACS Energy Lett.* **2020**, *5*, 540–544.

[39] J. J. Kaczur, H. Yang, Z. Liu, S. D. Sajjad, R. I. Masel, *Front. Chem.* **2018**, *6*, 263.

[40] M. Schalenbach, A. R. Zeradjanin, O. Kasian, S. Cherevko, K. J. Mayrhofer, *Int. J. Electrochem. Sci.* **2018**, *13*, 1173–1226.